Published by Institute of Physics Publishing for SISSA/ISAS

Received: *June 20, 2002*
Revised: *August 30, 2002*
Accepted: *September 2, 2002*

Gluon distribution functions in the $k_\perp$-factorization approach

Gösta Gustafson, Leif Lönnblad and Gabriela Miu

Dept. of Theoretical Physics
Sölvegatan 14A, S-223 62 Lund, Sweden
E-mail: Gosta.Gustafson@thep.lu.se, Leif.Lonnblad@thep.lu.se *and* Gabriela.Miu@thep.lu.se

Abstract: At small x, the effects of finite transverse momenta of partons inside a hadron become increasingly important, especially in analyses of jets and heavy-quark production. These effects can be systematically accounted for in a formalism based on $k_\perp$-factorization and unintegrated distribution functions. We present results for the unintegrated distribution function, together with the corresponding integrated one, obtained within the framework of the Linked Dipole Chain model. Comparisons are made to results obtained within other approaches.

Keywords: QCD, Deep Inelastic Scattering, Jets, Phenomenological Models.

Contents

1. Introduction

In the description of a given cross section in deeply inelastic lepton–hadron scattering (DIS), it is not enough to consider only the leading order perturbative terms. Although α_s may be small, each power of α_s may be accompanied by large logarithms due to the large phase space available for additional gluon radiation. It is, however, often possible to resum these emissions to all orders in the leading logarithmic approximation (LLA).

The most familiar resummation strategy is based on DGLAP [1, 2, 3, 4] evolution, which resums large logarithms of the virtual photon momentum transfer, Q^2. Within this formalism, the cross-section for any given physics process is calculated using collinear factorization of the form

$$\sigma(x, Q^2) = \sigma_0(x, Q^2) \sum_a \int \frac{\mathrm{d}z}{z} C^a(z)\, f_a\left(\frac{x}{z}, Q^2\right), \tag{1.1}$$

i.e. as a convolution of coefficient functions C^a and parton densities $f_a(x, Q^2)$.

DGLAP evolution describes most experimental results[1] from electron–proton and proton–proton colliders. By using input parton densities which are sufficiently singular when $x \to 0$, this formalism can also account for the strong rise of F_2 for small x, as observed at HERA. However, there are problems with the description of non-inclusive observables such as forward jet production in ep and heavy-quark production in ep and pp collisions.

[1] see e.g. [5] for a recent review.

In the region of very small x (asymptotically large energies), effects of finite transverse momenta of the partons may become more and more important. The appropriate description in this region of phase space is BFKL evolution [6, 7]. The cross-sections are calculated in the $k_\perp$-factorization approach of the form

$$\sigma(x, Q^2) = \int \frac{\mathrm{d}z}{z} \, \mathrm{d}^2 k_\perp \, \hat{\sigma}(z, Q^2, k_\perp^2) \, \mathcal{F}\left(\frac{x}{z}, k_\perp^2\right), \tag{1.2}$$

i.e. as a convolution over the energy fraction z and the transverse momentum $k_\perp$ of the incoming parton of off-shell partonic cross-sections $\hat{\sigma}$, and $k_\perp$-unintegrated parton densities,[2] $\mathcal{F}(x, k_\perp^2)$. This corresponds to a resummation of large logarithms of $1/x$. The BFKL evolution equation actually predicts a strong power-like rise of F_2 at small x.

Both the DGLAP and BFKL evolution were developed to describe inclusive quantities such as F_2, but they can be interpreted as an explicit summation of initial-state bremsstrahlung of quasi-real partons, and can thus, together with appropriately added final-state bremsstrahlung, also be used to describe exclusive multi-parton final states.

There exist a couple of models which take into account large logarithms of both Q^2 and $1/x$ in DIS. One such model, valid for both small and large x, has been developed by Ciafaloni, Catani, Fiorani and Marchesini, and is known as the CCFM model [8, 9]. The resulting unintegrated distribution functions, $\mathcal{F}(x, k_\perp^2, \overline{q})$, depend on two scales, the additional scale, $\overline{q}$, being a variable related to the maximum angle allowed in the emission. A problem with this approach is that the non-singular terms in the splitting function have not been included in a fully consistent way, and therefore CCFM does not fully reproduce the DGLAP result in the large Q^2 limit.

The Linked Dipole Chain model (LDC) [10, 11] is a reformulation and generalization of the CCFM model. It is based on the observation that the dominant features of the parton chains are determined by the subset of emitted gluons, which are ordered in both light-cone components, q_+ and q_-, and which significantly change the transverse momentum of the propagating gluon. This subset was called "primary" gluons, or the backbone of the chain. In LDC this subset of emissions is treated as initial state radiation, while all other emissions are treated as final state radiation. The result is that the evolution can be described by essentially single-scale dependent unintegrated distributions, $\mathcal{F}(x, k_\perp^2)$. However, as discussed further below, the $1/(1-z)$ pole in the splitting function does imply some dependence on the scale $\bar{q}$ also in the LDC formalism. It should be noted that the standard LDC formulation does not exactly reproduce the leading BFKL behavior for fixed coupling, but with a small modification almost identical results can be obtained (see section 2.3).

Like the DGLAP and BFKL equations, also the CCFM and LDC formalisms can be used to describe exclusive final states. To do this it is essential to add final state radiation in regions appropriate for the particular formalism used. In particular many gluons included as initial state radiation in the evolution chain in CCFM are added in a later phase as

[2] In this paper we will use $\mathcal{F}$ for the unintegrated parton distributions in general, and $\mathcal{G}$ for the unintegrated gluon distribution, treated as densities in $\log 1/x$, i.e. $\mathcal{G}(x) = xG(x)$. For the integrated ones we will use the standard notation f and g respectively.

final state radiation in LDC. Although very similar, this separation is also different in the BFKL and CCFM formalisms, as discussed in refs. [12] and [13]. These schemes give the same result only after soft collinear emissions have been included as final state radiation.

In this article we present results for the integrated and unintegrated gluon distribution functions obtained within the LDC formalism and make comparisons with the CCFM model and with results from other formalisms. The article is organized as follows. We start in section 2 by giving a short introduction to the DGLAP and BFKL formalisms for deeply inelastic *ep* scattering, moving over to a description of the CCFM model. We end this section with a somewhat more elaborate description of the Linked Dipole Chain model for DIS, which is implemented in the Monte Carlo event generator LDCMC [14]. This program can be used to describe both structure functions and exclusive properties of the hadronic final states.

As mentioned above the definition of the chains in the initial parton evolution is different in the different schemes. Therefore also the gluon distribution functions, which are not experimental observables, are not uniquely defined, but depend on the formalism used. We discuss this problem, and some different approaches presented in the literature, in section 3.

In section 4 we present our results for the unintegrated and integrated gluon distribution functions, obtained in the LDC formalism as implemented in LDCMC. These results are also compared to those of other approaches, and we discuss how to make relevant comparisons between the different formalisms.

We end this article with a summary in section 5.

2. Deep inelastic scattering

Typically a deeply inelastic scattering event is represented by a fan diagram, as the one shown in figure 1. The (quasi-)real emitted gluons, constituting the initial-state radiation, are labeled q_i, while the virtual propagators are referred to as k_i. The figure represents an exclusive final state, with the final-state radiation explicitly marked as the dashed lines. The final-state emissions have to be defined so that they do not affect the cross-section and give negligible recoils to the emitting partons. The exact separation between initial- and final-state radiation is not the same in the different formalisms discussed in the following subsections, and consequently the exclusive initial chains, as well as the distribution functions, are also different. This problem will be further discussed in sections 3 and 4.

We will here mostly discuss purely gluonic chains, which should give the dominating contributions at small x. We will use different approximations of the gluon splitting function $P_{\rm gg}(z) = \frac{1}{z} + \frac{1}{1-z} - 2 + z(1-z)$. Splitting a gluon means that we have two new gluons, carrying fractions z and $1-z$ of the original gluon energy, which contribute to the gluon density, while the contribution from the original one must be subtracted.

In analytical calculations of the distribution functions, the subtraction is achieved with the so-called plus prescription for the pole at $z = 1$ and the addition of a term proportional to $\delta(1-z)$ to the splitting function. At asymptotically small x, in the double leading logarithmic approximation, the distribution functions can be obtained by considering only the $1/z$ pole of the splitting function, thus effectively only adding one gluon, neglecting the recoil for the emitting mother gluon. In this way the problem with subtraction is avoided altogether. (Although less important for the qualitative properties, the non-leading terms are very essential for the quantitative results, e.g. for the power λ determining the increase for small x-values [10, 15, 16].)

The singularity at $z = 1$ is less important for the distribution functions, but if one is also interested in the properties of exclusive final states the effects of this pole cannot be neglected. When both poles are included in the splitting function the subtraction can be handled by a Sudakov form factor, which multiplies each splitting and represents the probability that the gluon to be split has not already been split before. Here *before* has to be defined by the ordering imposed on the emissions (e.g. $k_\perp$-ordering in DGLAP and angular ordering in CCFM). In an approximation where the non-singular terms in $P_{\rm gg}$ (i.e. the terms $-2 + z(1-z)$) are neglected, the Sudakov form factor, $\Delta_{\rm S}$, is given by

$$\ln \Delta_{\rm S} = -\int \overline{\alpha} \frac{dq_\perp^2}{q_\perp^2} \frac{dz}{1-z} \Theta_{\rm order}\,, \tag{2.1}$$

where $\overline{\alpha} = 3\alpha_s/\pi$. This definition is used in the CCFM approach. Equivalently the Sudakov form factor can be obtained by considering energy-momentum conservation [17] and be written

$$\ln \Delta_{\rm S} = -\int \overline{\alpha} \frac{dq_\perp^2}{q_\perp^2} z dz P_{\rm gg}(z) \Theta_{\rm order}\,. \tag{2.2}$$

Here the non-singular terms in $P_{\rm gg}$ can be included without problems, and this method is used in the LDCMC generator.

As mentioned above, the $1/(1-z)$ singularity and the associated Sudakov form factor are essential for the exclusive final state properties, but not equally important for the distribution functions. To simplify the notation and make the presentation more transparent, we will in the discussions in the rest of this section only include the effects of the $1/z$ pole. The effects of the remaining terms in the splitting function and the associated Sudakov form factor will instead be discussed in sections 3 and 4. In section 4 we will also consider the convolution of the perturbative evolution with non-perturbative input parton densities, which will also be ignored in the remainder of this section.

2.1 DGLAP and BFKL

In the DGLAP region, characterized by large Q^2 and limited $1/x$, the dominating contributions come from $k_\perp$-ordered chains which fulfill $Q^2 \gg k_{\perp n}^2 \gg k_{\perp,n-1}^2 \gg \cdots$ and $k_{+i} > k_{+,i+1}$. In the limit where also x is small, so that we can approximate the gluon splitting function with $P_{gg}(z) \approx 1/z$ (in the double leading log approximation — DLLA) we can write the unintegrated gluon distribution function for a fixed coupling α_s on the form

$$\begin{aligned} \mathcal{G}(x, k_\perp^2) &\sim \sum_n \int \prod^n \bar{\alpha} \frac{dx_i}{x_i} \frac{dk_{\perp i}^2}{k_{\perp i}^2} \theta(x_{i-1} - x_i) \theta(k_{\perp,i}^2 - k_{\perp,i-1}^2) \\ &\sim \sum_n \bar{\alpha}^n \frac{(\ln 1/x)^n}{n!} \frac{(\ln Q^2)^n}{n!} \approx \exp\left(2\sqrt{\bar{\alpha} \ln Q^2 \ln \frac{1}{x}}\right). \end{aligned} \tag{2.3}$$

where

$$\bar{\alpha} \equiv \frac{3\alpha_s}{\pi} \qquad \text{and} \qquad x_i \equiv \frac{k_{+i}}{P_{+,\,\mathrm{tot}}} \,. \tag{2.4}$$

In the case of a running coupling, $\overline{\alpha}(Q^2) \equiv \alpha_0/\ln Q^2$, we get the same exponential expression but with $\ln Q^2$ replaced by $\ln(\ln Q^2)$ and $\overline{\alpha}$ by α_0.

In the BFKL region of very small x and limited Q^2, chains that are not ordered in $k_\perp$ need to be accounted for, even though they are suppressed. The resulting unintegrated distribution function increases like a power at small x:

$$\mathcal{G} \sim \frac{1}{x^\lambda}\,\mathrm{f}(k_\perp, x)\,, \tag{2.5}$$

with the function $\mathrm{f}(k_\perp, x)$ describing a random walk in $\ln(k_\perp^2/\Lambda_{QCD}^2)$ [18, 19, 20, 11]. Such a power-like behavior is in approximate agreement with HERA data, with $\lambda \sim 0.3$. We note, however, that a corresponding increase is also obtained from NLO DGLAP evolution with appropriately adjusted input distribution functions.

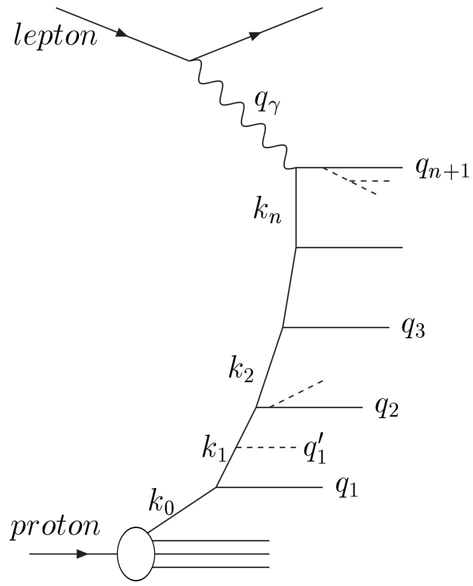

Figure 1: A fan diagram for a DIS event. The quasi-real partons from the initial-state radiation are denoted q_i, and the virtual propagators k_i. The dashed lines denote final-state radiation.

2.2 CCFM

The particular calculation scheme adopted by Ciafaloni, Catani, Fiorani and Marchesini has resulted in the well-known CCFM model [8, 9]. This model has been developed assuming purely gluonic chains. Further, only the singular terms in the splitting functions are included in a fully consistent way. Colour coherence implies that the initial-state emissions are ordered in angle (or equivalently in rapidity). According to the definition of the separation between initial- and final-state radiation, they are also ordered in the positive (along the incoming proton) light-cone momentum q_+. All other kinematically allowed emissions (symbolized by the q'_1 emission in figure 1) are defined as final-state emissions.

The CCFM model is based on the $k_\perp$-factorization formalism, and if we neglect the $1/(1-z)$ pole, the unintegrated distribution function in the small-x limit is given by

$$\begin{aligned}\mathcal{G}(x, k_\perp^2, \overline{q}) \sim \sum_n \int \prod^n \bar{\alpha} \frac{dz_i}{z_i} \frac{d^2 q_{\perp i}}{\pi q_{\perp i}^2} \Delta_{ne}(z_i, k_{\perp i}^2, \overline{q}_i) \times \\ \times\, \delta(x - \Pi z_i)\theta(\overline{q}_i - \overline{q}_{i-1} z_{i-1})\delta(k_\perp^2 - k_{\perp n}^2)\theta(\overline{q} - \overline{q}_n z_n)\,. \end{aligned} \tag{2.6}$$

The notation is that of figure 1, i.e. $q_{\perp i}$ and $k_{\perp i}$ are the transverse momenta of the real and virtual partons, respectively. The splitting parameter z is defined as $z_i = k_{+,i}/k_{+,i-1}$, and the so-called rescaled transverse momentum $\overline{q}_i$ is defined by $\overline{q}_i \equiv q_{\perp i}/(1 - z_i)$. The interval for the z-variables is between 0 and 1, which guarantees ordering in q_+, and the angular ordering condition is satisfied by the constraint

$$\overline{q}_i > \overline{q}_{i-1} z_{i-1} \,, \tag{2.7}$$

explicitely written out in eq. (2.6). Moreover, we note the occurrence of the so-called non-eikonal form factor $\Delta_{ne}(z, k_\perp^2, \overline{q})$ defined in ref. [9]. The distribution function, $\mathcal{G}$, depends on two separate scales, the transverse momentum, $k_\perp$, of the interacting gluon, and $\overline{q}$, which determines an angle beyond which there is no (quasi-) real parton in the chain of initial-state radiation. In the rest frame of the incoming proton, this limiting angle corresponds to a rapidity given by (if counted negative in the direction of the probe)

$$y_{\text{lim}} = \ln\left(x \frac{m_p}{\overline{q}}\right) . \tag{2.8}$$

In the original formulation there was also the so-called consistency constraint

$$k_{\perp i}^2 > z_i q_{\perp i}^2 \,, \tag{2.9}$$

which guarantees that the virtuality k^2 is well approximated by $-k_\perp^2$. The relevance of this constraint has been debated and has been disregarded in some analyses [21].

The CCFM evolution has been implemented in two hadron-level event generators, SMALLX [22, 23] and CASCADE [24] (which of course include also the $1/(1-z)$ pole), both maintained by Hannes Jung. These programs reproduce HERA data on F_2 well for small x, where purely gluonic chains should give the dominating contribution. For larger x, we expect a large contribution from valence quarks; such chains are not easily accounted for in the CCFM formalism and are not included in the programs.

Both programs are able to reproduce a wide range of final-state observables. We note, however, that there is a large sensitivity to uncertain non-leading corrections. In particular this is the case for forward-jet production at HERA. The non-singular terms in the gluon splitting function can not be included in a fully consistent way, and they are not included in the original CCFM formulation. With this version of the MC the experimental forward-jet rates are well described. If, however, the non-singular terms are included in an approximate way, which would be a more natural option, the jet rates come out approximately a factor two below the data [5].

2.3 The linked dipole chain model

The Linked Dipole Chain model (LDC) is also formulated in terms of $k_\perp$-factorization and unintegrated distribution functions. It is a reformulation and generalization of the CCFM model, in which the separation between initial state bremsstrahlung (ISB) and final state bremsstrahlung (FSB) has been modified. This results in a more simple description, with the unintegrated distribution functions being (essentially) dependent on only one scale and allowing for some sub-leading corrections to be introduced in a rather straight-forward manner.

The LDC model is based on the observation that the dominant features of the parton chains are determined by the subset of emitted gluons, which is ordered in both light-cone components, q_+ *and* q_-, (which implies that they are also ordered in angle or rapidity y) and with $q_{\perp i}$ satisfying the constraint

$$q_{\perp i} > \min(k_{\perp i}, k_{\perp,i-1})\,. \tag{2.10}$$

In LDC this subset (called "primary" gluons, or the backbone of the chain) forms the chain of initial state radiation, and all other emissions are treated as final state radiation.

This redefinition of the ISB–FSB separation implies that one single chain in the LDC model corresponds to a set of CCFM chains. As was shown in ref. [10], when one considers the contributions from all chains of this set, with their corresponding non-eikonal form factors, they just add up to one. Thus, the non-eikonal form factors do not appear explicitly in LDC. The result is a simpler form for the unintegrated distribution functions, $\mathcal{F}(x, k_\perp^2)$, which essentially depend only on a single scale, $k_\perp^2$. Since many of the gluons which make up the initial-radiation chain in the CCFM model, are treated as final-state radiation in the LDC formalism, typical z-values are smaller in the LDC model and most of the problem of angular ordering is postponed to the treatment of the final-state radiation. However, as discussed further below, the $1/(1-z)$ pole in the splitting function does imply some dependence on the scale $\bar{q}$ also in the LDC formalism.

Again keeping only the $1/z$ pole, we find for the gluon distribution in the LDC formalism

$$\mathcal{G}(x, k_\perp^2) \sim \sum_n \int \prod^n \bar{\alpha} \frac{dz_i}{z_i} \frac{d^2 q_{\perp i}}{\pi q_{\perp i}^2} \theta(q_{+,i-1} - q_{+i}) \theta(q_{-i} - q_{-,i-1}) \delta(x - \Pi z_i) \delta(\ln k_\perp^2 - \ln k_{\perp n}^2)\,. \tag{2.11}$$

The notation in the above and what will follow refers to that of figure 2. Here, a typical DIS event is shown together with the corresponding phase space available in the γ-p rest frame, where the rapidity, y, and the transverse momentum, $q_\perp$, of any final-state parton are limited by a triangular region in the $(y, \ln q_\perp^2)$-plane. The proton direction is towards the right end of the triangle, and the photon direction is towards the left. The real emitted (ISB) gluons are represented by points in this diagram. The virtual propagators do not have well defined rapidities, and are represented by horizontal lines, the left and right ends of which have the coordinates $(\ln[k_{+i}/k_{\perp i}], \ln k_{\perp i}^2)$ and $(\ln[-k_{\perp i}/k_{-i}], \ln k_{\perp i}^2)$ respectively. The phase space available for FSB is given by the area below the horizontal lines (including the folds that stick out of the main triangle).

The fact that the dominant properties of the evolution are determined by the subset of "primary" emissions has been further studied in ref. [12], where they are called k-changing gluons. That paper also discusses the effect of emissions close to the boundary of the constraint in eq. (2.10), which are important for single logarithmic accuracy. In fact, with the constraint (2.10) LDC does not exactly reproduce the BFKL result. An almost identical value for the power λ, determining the increase for small x, is, however, obtained by the modified cut $q_{\perp i} > \sqrt{k_{\perp i} \cdot k_{\perp,i-1}}$ (in leading order for fixed α_s) [25].

Due to the different separation between ISB and FSB, it is important to include final state emissions before a comparison between exclusive final states in LDC and CCFM or BFKL. For a comparison between the final states obtained in CCFM and BFKL see refs. [12, 13].

JHEP09(2002)005

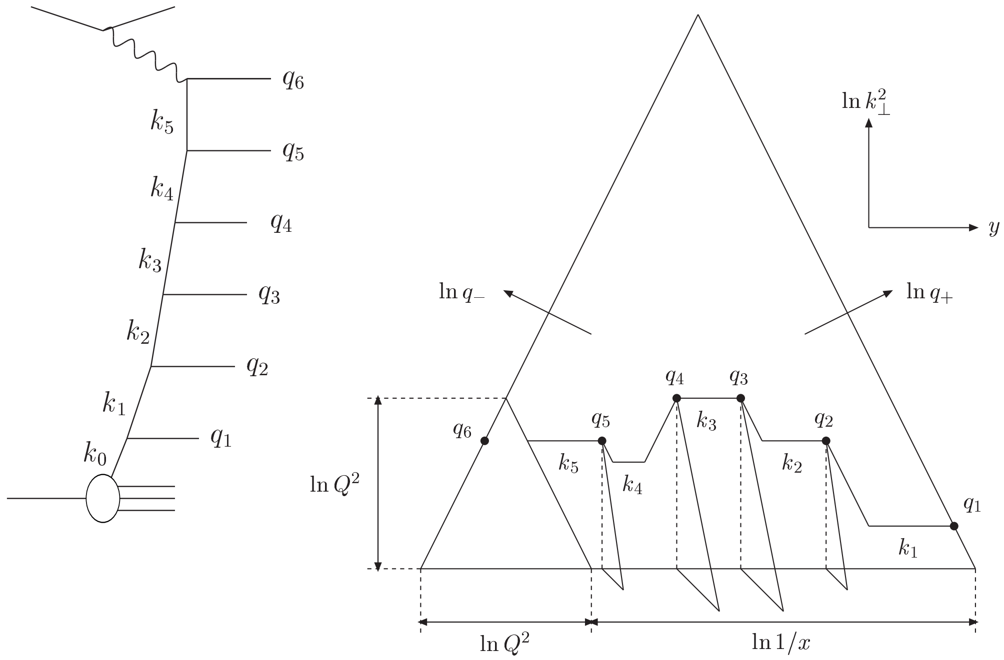

Figure 2: The initial-state emissions q_i in the $(y, \kappa = ln(k_\perp^2))$-plane. Final-state radiation is allowed in the region below the horizontal lines. The height of the horizontal lines determine $\ln k_{\perp i}^2$. The light-cone momenta k_{+i} and k_{-i} can be read off as described in the text.

The ordering of the CCFM evolution in q_+ but not in q_- means that this formalism is not left–right symmetric. In contrast the LDC formulation is completely symmetric, which implies that the chain in figure 2 can be thought of as evolved from either the photon or the proton end. (Thus, the LDC formalism automatically takes into account contributions from “resolved virtual photons”.)

Returning to eq. (2.11), we note that it can equally well be expressed in terms of the virtual propagator momenta. Due to the condition in eq. (2.10) we have $q_{\perp i}^2 \approx \max(k_{\perp i}^2, k_{\perp,i-1}^2)$ and, suppressing the θ- and δ-functions, we obtain

$$\mathcal{G} \sim \sum \int \prod \bar{\alpha} \frac{dz_i}{z_i} \frac{dk_{\perp i}^2}{\max(k_{\perp i}^2, k_{\perp,i-1}^2)} \,. \tag{2.12}$$

In particular we note that this implies that, for a “step up” or a “step down” in $k_\perp$, the following weights result:

$$\frac{d^2 q_{\perp i}}{q_{\perp i}^2} \approx \frac{d^2 k_{\perp i}}{k_{\perp i}^2} \,, \qquad k_{\perp i} > k_{\perp,i-1} \tag{2.13}$$

and

$$\frac{d^2 q_{\perp i}}{q_{\perp i}^2} \approx \frac{d^2 k_{\perp i}}{k_{\perp i}^2} \cdot \frac{k_{\perp i}^2}{k_{\perp,i-1}^2} \,, \qquad k_{\perp i} < k_{\perp,i-1} \,. \tag{2.14}$$

Thus, for a step down there occurs an additional suppression factor $k_{\perp i}^2 / k_{\perp,i-1}^2$.

The relation between the integrated and the unintegrated distribution functions are symbolically written as $xf(x, Q^2) \sim \int \frac{dk_\perp^2}{k_\perp^2} \mathcal{F}(x, k_\perp^2)$. The exact relationship is somewhat dependent on the evolution scheme used for $\mathcal{F}(x, k_\perp^2)$. For LDC we have

$$xf(x, Q^2) = \int^{Q^2} \frac{dk_\perp^2}{k_\perp^2} \mathcal{F}(x, k_\perp^2) + \int_{Q^2} \frac{dk_\perp^2}{k_\perp^2} \mathcal{F}\left(x\frac{k_\perp^2}{Q^2}, k_\perp^2\right) \frac{Q^2}{k_\perp^2}, \tag{2.15}$$

assuming a single-scale dependent unintegrated distribution function.

The first term of eq. (2.15) corresponds to chains whose struck parton is less virtual than the probe, $k_\perp^2 < Q^2$. The second term contains the suppressed contributions that come from chains whose struck parton has $k_\perp^2 > Q^2$; the suppression factor $Q^2/k_\perp^2$ is analogous to the one occurring in eq. (2.14). Note also that the x-argument in the unintegrated distribution function of the second term has been rescaled by the factor $k_\perp^2/Q^2$.

Below we list some properties of the LDC model:

- The natural scale in the running coupling, α_s, is $q_{\perp i}^2$, which coincides with $\max(k_{\perp i}^2, k_{\perp, i-1}^2)$.
- Non-leading effects such as those coming from quark-initiated chains, from the non-singular terms in the splitting functions and from energy-momentum conservation can be included in a straight-forward manner. It is also possible to correct the two emissions connected with the highest-virtuality link with the full $2 \to 2$ matrix element, thus improving the result. Finally, for the ISB emission closest to the photon end, the full off-shell $\mathcal{O}(\alpha\alpha_s)$ matrix element is used.
- The fact that fewer gluons are considered as initial-state radiation implies that typical z-values are smaller, thus resulting in smaller sub-leading corrections.
- The formalism is greatly simplified by the fact that the non-eikonal form factors do not appear explicitly in the model.
- The LDC formalism is fully left-right symmetric, in the sense that the result is independent of whether the evolution starts at the probe (photon) or target (proton) end. Hence it can easily be generalized to the case when the photon is replaced by a hadron. As a result, the formalism can be applied to the study of jet production in hadronic collisions [26, 27].
- Besides giving an inclusive description of the events, the result in eq. (2.12) (modified to include also the remaining terms of the splitting function) can also be interpreted as the production probability for an exclusive final state.

These qualities make LDC particularly suitable for implementation in an event generator. One such LDC-based Monte Carlo event generator, LDCMC, has been developed by Kharraziha and Lönnblad [14].

The LDCMC has been shown to be able to reproduce available F_2 data very well (see further section 4), not only the small-x data from of HERA but also data at higher x from fixed target experiments. This success relies on the fact that quark-initiated chains are easily incorporated in the evolution.

It should be mentioned that, just like the CCFM-based CASCADE, LDCMC has problems describing the H1 forward-jet data. Again the data can be reproduced only when the non-singular terms of the gluon splitting function are omitted. The more physical case of including the full splitting function predicts a distribution which is approximately a factor 2 below the data.

In section 4 we present results for the integrated and unintegrated gluon distribution functions obtained within the LDC formalism using the LDCMC simulation program. Before comparing these results with those of other approaches, we discuss in the following section the relationship between the integrated and unintegrated distribution functions in different formalisms.

3. Discussion on different distribution function definitions

In contrast to the structure function F_2, the unintegrated parton distributions are not experimental observables, and therefore depend on the specific scheme in which they are defined. The parton distribution functions and the hard sub-collision cross sections $\hat{\sigma}$ have to be defined consistently, so that the convolution in eq. (1.2) gives the experimentally observable cross section. It has also been argued that the unintegrated distributions are not gauge-invariant objects, which implies that there is a dependence on the gauge choice used for the off-shell matrix elements in the convolution.[3]

For asymptotically large values of Q^2 or $1/x$ it is possible to define unintegrated parton distribution functions, $\mathcal{F}(x, k_\perp^2)$, which depend on a single scale, $k_\perp^2$, specifying the transverse momentum (or virtuality) of the interacting parton. In the DGLAP region the $k_\perp$-ordering of the links implies that we can define $\mathcal{F}(x, k_\perp^2)$ as the derivative of the integrated distribution functions, $xf(x, Q^2)$, and thus

$$xf(x, Q^2) = \int^{Q^2} \frac{dk_\perp^2}{k_\perp^2} \mathcal{F}(x, k_\perp^2)\,. \tag{3.1}$$

Also in the BFKL equation the distribution functions are determined by a single scale. However, since the chains are not ordered in $k_\perp$, the integrated distribution function, $f(x, Q^2)$, also obtains contributions from $k_\perp$-values larger than Q^2, and therefore the simple relation in eq. (3.1) is not satisfied.

As discussed in section 2.2 the angular ordering in the CCFM model implies that the unintegrated distribution functions depend on two scales, $k_\perp$ and $\overline{q}$, where $\overline{q}$ specifies the limiting angle in eq. (2.8). (Note that the strong ordering in $k_\perp$ in DGLAP, or in x in BFKL, also automatically implies an ordering in angle, which makes this second scale redundant.) Varying this angular constraint has two effects:

(*a*) Increasing $\overline{q}$ implies additional contributions from chains with one (or more) emissions with rapidity in the now allowed angular range. These chains give a positive contribution to the distribution function. We also note that, as the chains have to end with transverse momentum $k_\perp$, most of them will have $q_\perp \lesssim k_\perp$, where $q_\perp$ is the transverse momentum of the emission in the new angular region.

[3] See e.g. discussions in [5] and [28].

(*b*) Emission of an extra gluon with $q_\perp > k_\perp$ will change the $k_\perp$ of the active gluon. This will give a negative contribution, which is described by a Sudakov form factor.

For large values of $\overline{q}$ the suppression from the Sudakov dominates, and $\mathcal{G}(x, k_\perp^2, \overline{q})$ decreases with increasing $\overline{q}$ for fixed x and $k_\perp$. However, for $\overline{q} \lesssim k_\perp$ the first effect dominates, and $\mathcal{G}$ increases with $\overline{q}$. In the CCFM formalism this dependence on $\overline{q}$ for fixed x and $k_\perp$ is very strong, when $\overline{q}$ varies in the neighborhood of $k_\perp$. The angular constraint is expressed by the last θ-function in eq. (2.6), which guarantees the relation

$$\overline{q} > \overline{q}_n z_n\,, \qquad \text{where } \overline{q}_n \equiv \frac{q_{\perp n}}{1 - z_n}\,. \tag{3.2}$$

This implies an upper limit for z_n of the last emission given by

$$z_n < z_{\text{lim}} = \frac{\overline{q}}{\overline{q} + q_\perp}\,. \tag{3.3}$$

From this result we can see that if the scale $\overline{q}$ is chosen in the neighborhood of $k_\perp$, then a large fraction of the possible chains are cut away. To realize this we make two observations:

(i) For $\overline{q} = k_\perp$ we find $z_{\text{lim}} \approx 0.5$ when the last link is a step up in $k_\perp$ (in which case $q_\perp \approx k_\perp$), and $z_{\text{lim}} < 0.5$ when the last link is a step down (and $q_\perp > k_\perp$).

(ii) In the CCFM model the $1/z$ pole in the splitting function is screened by the non-eikonal form factor, and the z-distribution obtained in the SMALLX and CASCADE MCs therefore does not peak at small z-values, but has a maximum around $z = 0.5$ [5].

This implies that for $\overline{q} = k_\perp$ the constraint in eq. (3.3) will exclude a large fraction of the possible chains. Furthermore, the fact that for $\overline{q} = k_\perp$, z_{lim} approximately coincides with the maximum in the z-distribution implies that increasing (decreasing) $\overline{q}$ in the neighborhood of $k_\perp$ includes (excludes) a significant set of chains. Consequently, for fixed $k_\perp$, the structure functions depend strongly on $\overline{q}$ in this region. As we will see in the next section, $\mathcal{G}(x, k_\perp^2, \overline{q})$ approximately saturates when $\overline{q}$ approaches $2k_\perp$, before it decreases for very large $\overline{q}$-values.

A similar angular constraint can be introduced also in the LDC formalism, giving distribution functions depending on two separate scales. However, many emissions with $q_\perp < k_\perp$, which are treated as initial-state emissions in CCFM, are treated as final-state emissions in LDC. Typical z-values are smaller, since small z are not screened by a non-eikonal form factor. Therefore such a constraint on the initial state emissions has a smaller effect in LDC than in the CCFM scheme, and the LDC distributions vary much more slowly with $\overline{q}$ in the region $q_\perp \lesssim k_\perp$.

The quantities of primary interest are not the unobservable parton distributions, but the cross sections for physical processes, where the parton distribution is convoluted with a hard parton-parton sub-collision, $\hat{\sigma}$. A Sudakov suppression as in point (b) above, for the evolution between the virtuality of the active parton and the scale of the hard sub-collision, could in principle be included in either the distribution functions or in $\hat{\sigma}$. It is, however, not normally included in calculations of $\hat{\sigma}$, and it is therefore more natural to include it in the distribution functions. In the LDC formalism, the relevant scale should then correspond to a limiting angle given by the final state partons in the hard collision. It is easy to show that using the parton (colour-) connected to the incoming one implies

$$\overline{q}^2 = \frac{\hat{t}\hat{s}}{\hat{u}} \tag{3.4}$$

where $\hat{t}$, $\hat{s}$, and $\hat{u}$ are the Mandelstam variables for the sub-collision. Thus if $\hat{s}$ is large compared to $\hat{t}$ we find $\overline{q}^2 \approx -\hat{t}$. For a very hard collision we find $\overline{q}^2$ of the same order as $\hat{s}$. In the CCFM formalism this choice would according to point (a) above exclude contributions with softer emissions in between the two partons produced in the hard collision (and somewhat underestimate the result). An alternative choice would be $\overline{q}^2 = \hat{s}$, which corresponds to a limiting angle equal to 90° in the rest frame of the hard sub-collision. This would then include a Sudakov suppression between $\hat{t}$ and $\hat{s}$, and thus possibly give a slight underestimate. This may, however, not be a very big problem. The important point is that the scale $\overline{q}$ should be determined by the scales in the hard sub-collision, which normally are substantially larger than $k_\perp$. As we will see in the following section, in the range $\overline{q} \sim 2k_\perp$ the variation with $\overline{q}$ is not dramatic, and actually it turns out that here the different schemes will give rather similar results.

Many other schemes are presented in the literature to treat unintegrated parton distributions. Besides with the CCFM formalism in the CASCADE and SMALLX MCs, which in the following will be referred to as JS (Jung and Salam) [29], we compare in the following section our results also with the formalisms presented by Kwiecinski, Martin, and Stasto (KMS) [30] and by Kimber, Martin, and Ryskin (KMR) [31]. In KMS a term describing leading order DGLAP evolution is added to the BFKL equation. The parton distribution is described by a single scale, $k_\perp$, and is assumed to satisfy the relation in eq. (3.1). In KMR two-scale parton distributions are extracted from the same unified DGLAP-BFKL evolution equation, but the angular constraint is imposed on the last link in the chain. As the value of $\overline{q}$ only puts a limit on the last emission, the dependence on $\overline{q}$ is significantly weaker than in the CCFM model. Finally we will compare to a simple derivative, according to eq. (3.1), of the integrated gluon density from the GRV98 [32] parameterization, referred to as dGRV in the following.

4. Results

In this section we discuss some results obtained from LDCMC. To illuminate the effect of the different contributions we study the following three different versions:

1. *Standard*: Including non-leading contributions from quarks and non-singular terms in the splitting functions.

2. *Gluonic*: Including non-singular terms in the splitting functions, but no quark links in the evolution.

3. *Leading*: Also purely gluonic chains, but with only the singular terms in the gluon splitting function.

fit	A_g	a_g	b_g	a_d	b_d	a_u	b_u	a_s	b_s	$k_{\perp 0}$	$\int xg(x)$	χ^2/d.o.f.
standard	1.86	**0**	**4**	1.78	**3**	0.57	**3**	**0**	**4**	0.99	*0.37*	694/625
gluonic	2.71	**0**	**4**							1.80	*0.54*	193/86
gluonic-2	3.11	**0**	**7**							2.17	*0.39*	125/86
leading	2.34	**0**	**4**							1.95	*0.47*	126/86

Table 1: The result of the fit of the parameters for the input parton densities. The *standard* version has been fitted to data from H1 [33], ZEUS [34], NMC [35] and E665 [36] in the region $x < 0.3$, $Q^2 > 1.5\,\mathrm{GeV}^2$, while the *gluonic* and *leading* have been fitted to H1 data only, in the region $x > 0.013$ and $Q^2 > 3.5\,\mathrm{GeV}^2$. The last two columns give the resulting fraction of the proton momentum carried by the gluons and the χ^2 over the number of fitted data points, respectively. Parameters in bold face have not been fitted.

To get realistic results from these three versions we now also need to consider the convolution of non-perturbative input parton densities. These are not à priori known, but need to be parameterized in some way. We will use the same parameterization as in [14] given by

$$xf_i(x, k_{\perp 0}^2) = A_i x^{a_i}(1-x)^{b_i}\,, \tag{4.1}$$

where $i = d_v, u_v, g$ and s for the d-valence, u-valence, gluon and sea-quark densities respectively (where the sea flavour densities are assumed to be $f_{\bar{d}} = f_{\bar{u}} = 2f_{\bar{s}}$). The parameters A_i, a_i, b_i and the perturbative cutoff, $k_{\perp 0}$, are then fitted to reproduce the measured data on F_2. There are some sum rules which fix the relationship between some of the parameters. The A_{d_v} and A_{u_v} are fixed by flavour conservation and A_s is fixed by momentum conservation. The fits to F_2 do not constrain the remaining parameters very strongly, so we have fixed the b parameters to 3 in the valence densities and to 4 in the sea and gluon densities. We have also chosen to fix $a_g = a_s = 0$. To check the sensitivity to the b parameter we have an additional fit for the *gluonic* case with $b = 7$ called *gluonic-2*. In table 1 we present the result of the fits. Note that in the case of the *gluonic* and *leading* versions, only the gluon input density is considered.

In figure 3 we show the resulting reproduction of F_2 data. Clearly, all versions give a satisfactory fit to the data. The *standard* version gives an excellent description for all values of x. The *gluonic* and *leading* versions are naturally unable to fit the large-x data, as the inclusion of quark-initiated chains is essential for a description of large x-values. These versions are therefore only fitted to the small-x H1 data, and these fits are shown separately in figure 3b. We note that *gluonic-2* gives a better fit than *gluonic*, but we will anyway in the following concentrate on the latter, to make the comparison with the JS results (which also uses $b_g = 4$) more informative.

It should be noted that the version of LDCMC used here has not been released yet, and differs somewhat from the one described in [14]. The main difference is the handling of the Sudakov form factors, which were not quite correct in the original version. Also the full off-shell $\gamma^* g^* \to q\bar{q}$ matrix element is now included.[4] These, and other minor changes, do not give a big effect on the results.

[4] Note, however, that the matrix element in [37] is used, rather than the one from [38] used in SMALLX and CASCADE.

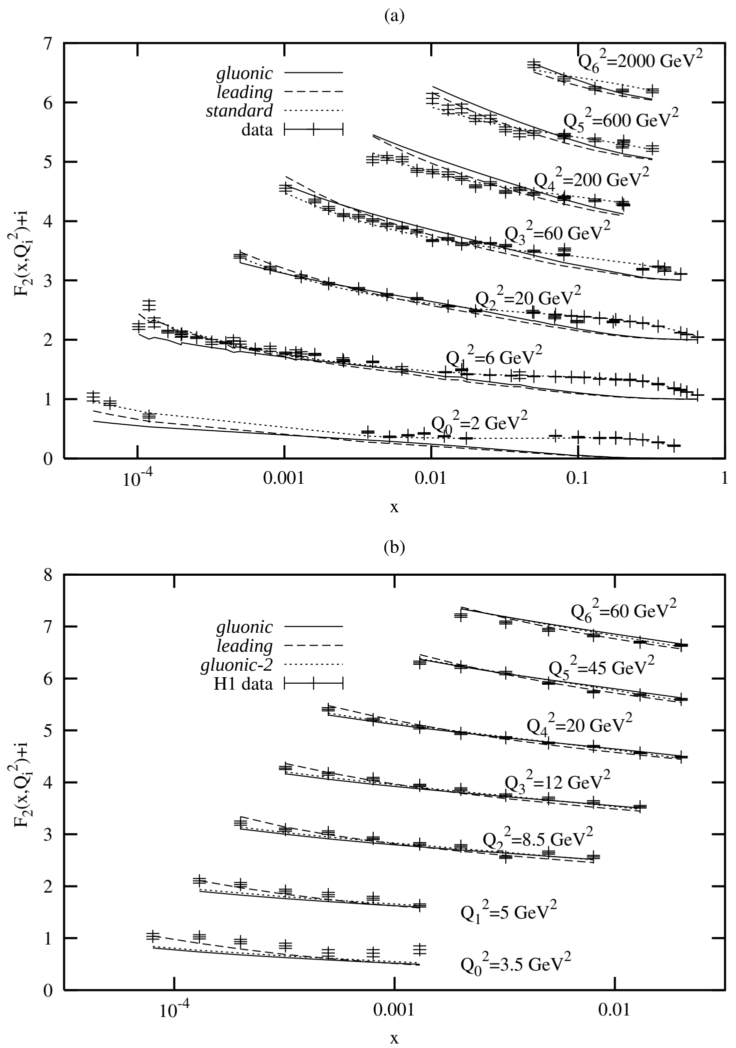

Figure 3: The description of F_2 data as a function of x for the different fits presented in this paper. To separate the results for different Q^2, what is shown is $F_2 + i$ for Q_i^2. In (a) both small and large x data from H1, ZEUS [34], NMC [35] and E665 [36] are included. The full line is *gluonic*, dashed is *leading* and the dotted line is *standard*. In (b) the versions with only gluonic chains are compared to small-x H1 data [33]. As in (a), full line is the *gluonic* case, dashed is *leading*, whereas dotted is *gluonic-2* (with b_g=7).

In the following subsections we discuss the corresponding results for the integrated and the unintegrated gluon distribution functions. As we will see, the results are very similar for the *standard* and the *gluonic* version. The differences in the cascade can here be compensated by the adjustment of the input distribution functions and the perturbative cutoff, $k_{\perp 0}$. For the *leading* version, without the non-singular terms in the splitting function, we find, however, that the resulting differences are small but not negligible.

4.1 Results for the integrated gluon distribution function

We start by studying the results obtained for the integrated gluon distribution function.

JHEP09(2002)005

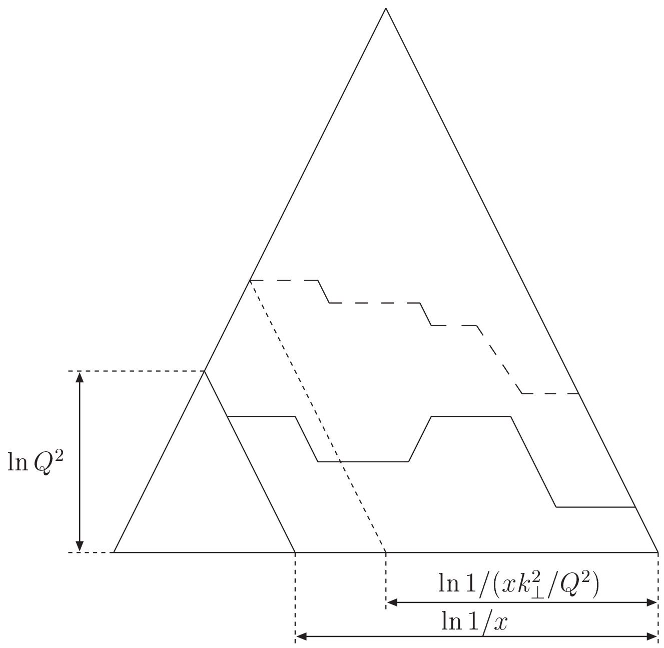

Figure 4: The hard colour-neutral probe Q^2 probes the gluon. The continuous line and the long-dashed line chains correspond to a struck gluon of $k_\perp^2 < Q^2$ and $k_\perp^2 > Q^2$, respectively.

As mentioned in section 2.3 (cf. eq. (2.15)), in the LDC model the relation between the integrated and the unintegrated gluon distribution functions is as follows:

$$xg(x,Q^2) = \int_{k_{\perp 0}^2}^{Q^2} \frac{dk_\perp^2}{k_\perp^2} \mathcal{G}(x,k_\perp^2,Q) + \int_{Q^2}^{Q^2/x} \frac{dk_\perp^2}{k_\perp^2} \mathcal{G}\left(x\frac{k_\perp^2}{Q^2},k_\perp^2,Q\right)\frac{Q^2}{k_\perp^2} + xg_0(x,Q_0^2)\times\Delta_{\mathrm{S}}\,. \tag{4.2}$$

Thus, the integrated distribution function receives contributions from three different terms. The first term corresponds to struck gluons of transverse momenta below the virtuality of the probe, $k_\perp^2 < Q^2$ (the full line in the triangular phase space of figure 4 is an example of such a chain), while the second term originates from chains whose struck gluons have $k_\perp^2 > Q^2$ (e.g. the long-dashed line in figure 4). Finally, the third term is the contribution from the input distribution function, corresponding to the case when no evolution has taken place.

As discussed in sections 2.3 and 3, the distribution function $\mathcal{G}(x,k_\perp^2,Q)$ in the LDC model depends only very weakly upon the scale Q. This dependence is due to the Sudakov form factor corresponding mainly to the $1/(1-z)$ term in the splitting function. Although this dependence is weak and can essentially be neglected in the first two terms in eq. (4.2), it has a larger effect on the last term, where it is explicitely included as a multiplicative factor. This term dominates at large x, and the effect of the form factor is a suppression for larger values of Q^2.

We first study the relative importance of the different terms contributing to the LDC integrated gluon distribution function. In figure 5 the integrated gluon distribution function is shown as a function of x, for fixed $Q^2 = 16\,\mathrm{GeV}^2$. As can be seen, at small x-values the

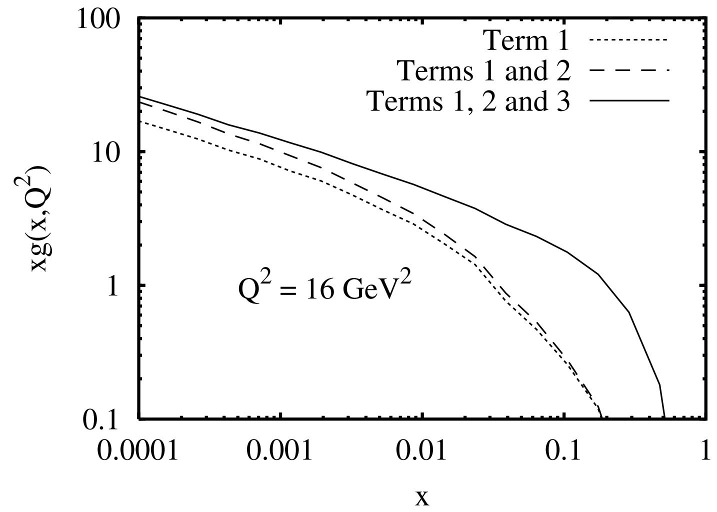

Figure 5: Relative importance of the different terms contributing to the LDC integrated gluon distribution function, for fixed $Q^2 = 16\,\mathrm{GeV}^2$. The dotted curve corresponds to keeping only the first term in eq. (4.2); keeping the first and second terms we obtain the dashed curve. The total result is represented by the full curve.

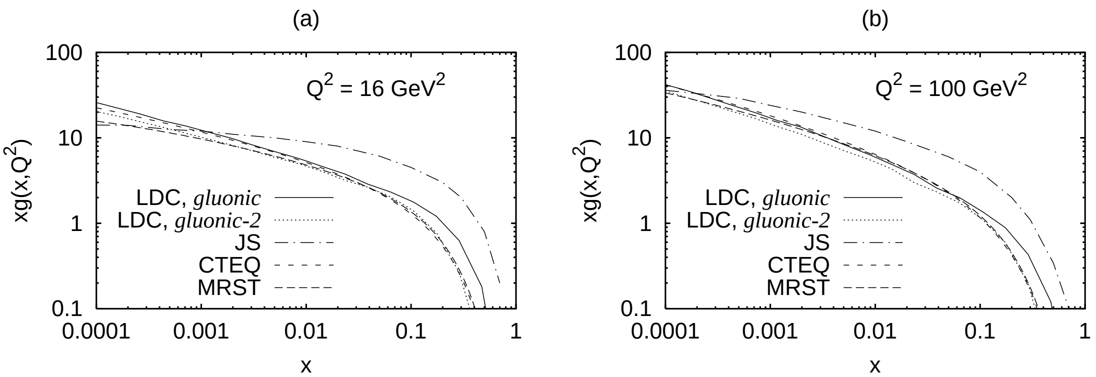

Figure 6: The LDC integrated gluon distribution function (full curve is *gluonic*, dotted curve is *gluonic-2*), compared to the corresponding results of JS (dash-dotted curve), CTEQ (short-dashed curve) and MRST (long-dashed curve), for (a) $Q^2 = 16\,\mathrm{GeV}^2$ and (b) $Q^2 = 100\,\mathrm{GeV}^2$.

first term of eq. (4.2) dominates; as x decreases the second term becomes noticeable. At large x-values, the behavior is governed by the input distribution function.

Next we compare the LDC results with those obtained by other analyses. In figure 6 we show the LDC integrated gluon distribution function as a function of x for $Q^2 = 16\,\mathrm{GeV}^2$ and $Q^2 = 100\,\mathrm{GeV}^2$. We show our result for the *gluonic* together with the *gluonic-2* case. As discussed above, they both give a good fit to F_2. We see that the LDCMC results lie significantly below the JS curve for large x, but above JS for smaller x-values.

Also shown in figure 6 are the corresponding results for CTEQ5M1 [39] and MRST20011 [40]. An important point is that, while the LDC and JS results have been fitted to F_2 data only, the CTEQ and MRST curves have been fitted to more data. We see that these latter

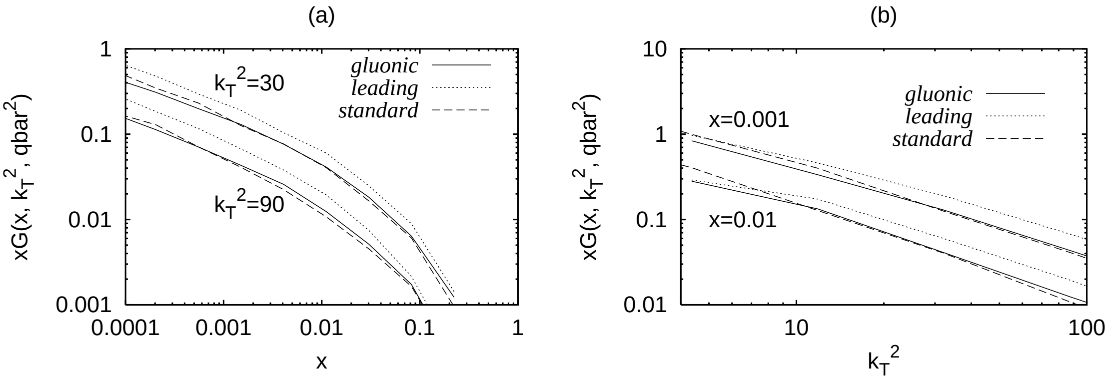

Figure 7: The LDC unintegrated gluon distribution function as a function of (a) x and (b) $k_\perp^2$. Study of sub-leading effects caused by inclusion of quarks and non-singular terms in the gluon splitting function. Full line is *gluonic*, dotted line is *leading* and dashed line is *standard*. (In these figures $\overline{q}$ is put equal to $k_\perp$.)

curves are more or less in agreement at large x, where there is more data available, while they separate more for smaller x-values. Clearly the LDC result agrees well with these curves for small x, where it almost coincides with CTEQ5M1. For larger x the LDC curve lies above CTEQ and MRST for *gluonic*, but agrees well with them for *gluonic-2*.

This comparison leads to increased confidence in the physical relevance of the LDC model in general and in the LDC unintegrated gluon distribution function in particular. We shall study this in the next subsection.

4.2 Results for the unintegrated gluon distribution function

We now turn our attention to the topic of unintegrated gluon distribution functions, and we first want to study the effects from sub-leading corrections caused by the inclusion of quarks and by the inclusion of the non-singular terms in the gluon splitting function, in order to verify the statements made earlier in this section.

In figure 7 the unintegrated LDC gluon distribution function is shown both as a function of x and $k_\perp^2$. Comparing the result for the purely gluonic case to that when we allow for quarks as well, we see that the differences are very small. (Note that the input distribution functions have been refitted.) Even though the effect of omitting the non-singular terms in the gluon splitting function is rather small, it is nevertheless not completely negligible: as can be seen in figure 7a, at small x there is a discrepancy of about a factor of two, a result that is related to the problem with the description of H1 forward-jet data that was mentioned in section 2.

Our conclusion is that the non-leading effects can be largely compensated by slight modifications of the input distribution functions; we note in particular that the results with and without quark links are almost identical.

We note that there is a slight drop in the *gluonic* and *leading* curves for small $k_\perp^2$ in figure 7b (this is also visible in some of the following figures). This is due to the rather high cutoff used for these fits and because the input distribution is treated as a delta function at

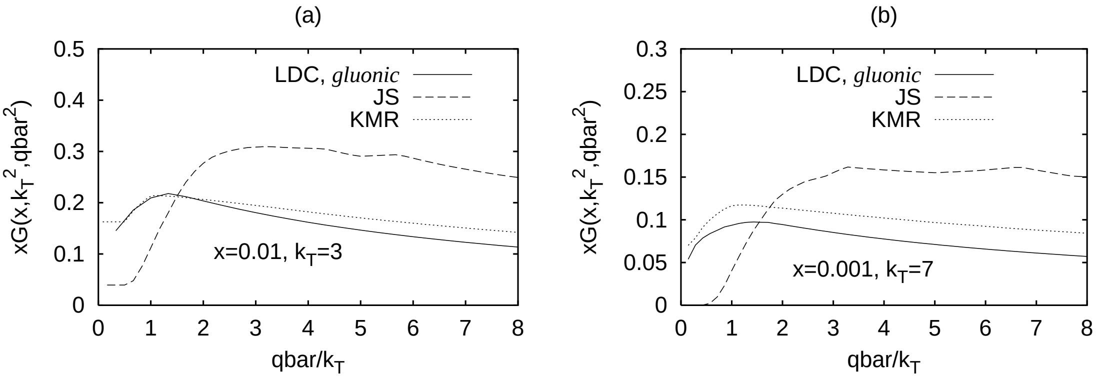

Figure 8: The LDC *gluonic* unintegrated gluon distribution function (full curve), compared to the corresponding results of JS (long-dashed curve) and KMR (dotted curve), as functions of $\overline{q}/k_\perp$ for (a) $x = 0.01$ and $k_\perp = 3\,\text{GeV}$ and (b) $x = 0.001$ and $k_\perp = 7\,\text{GeV}$.

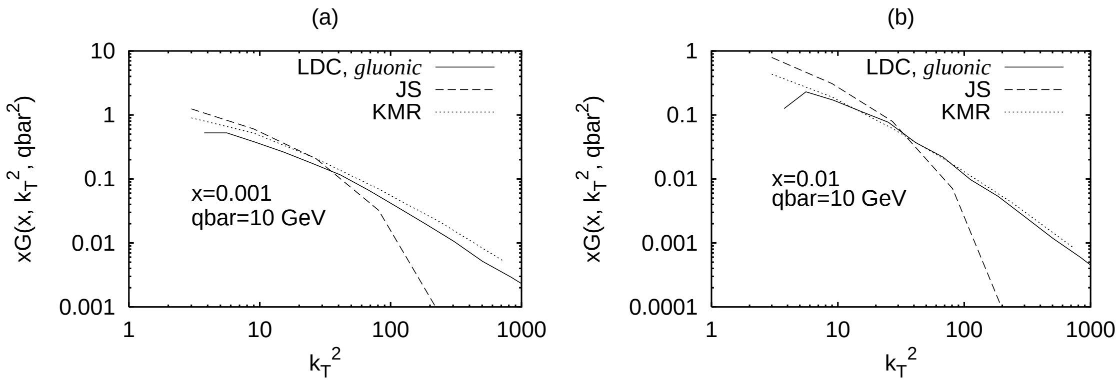

Figure 9: The LDC *gluonic* unintegrated gluon distribution function (full curve), compared to the corresponding results of JS (long-dashed curve) and KMR (dotted curve), as functions of $k_\perp^2$ for (a) $x = 0.001$ and (b) $x = 0.01$. (In these figures $\overline{q}$ is put equal to $10\,\text{GeV}$.)

$k_\perp = 0$. In the JS, KMR and KMS approaches, the input gluon is added with a gaussian distribution in $k_\perp$.

We now want to study the dependence upon the two different scales discussed in section 3. We show in figure 8 the dependence on $\overline{q}$ for fixed $k_\perp$ for the LDC, CCFM, and KMR formalisms. As discussed in section 3, the $\overline{q}$-dependence is relatively weak in the LDC model, but very strong in the CCFM approach. We also see that the result in the KMR formalism is quite insensitive to variations in $\overline{q}$, and rather similar to the LDC results. This is also illustrated in figure 9, which shows the results as functions of $k_\perp^2$ for fixed $\overline{q} = 10\,\text{GeV}$. We see that the JS results start to fall dramatically below the other two, as $k_\perp$ approaches $\overline{q}$.

From figure 8 we note, however, that the CCFM result appears to saturate for $\overline{q} \gtrsim 2k_\perp$, before it falls off for large values of $\overline{q}/k_\perp$. In a hard-interaction event the scales $|\hat{t}|$ and $\hat{s}$ are normally larger than $k_\perp^2$, and often characteristically by a factor of this order. For this reason we want to argue that when comparing the different formalisms, it is more

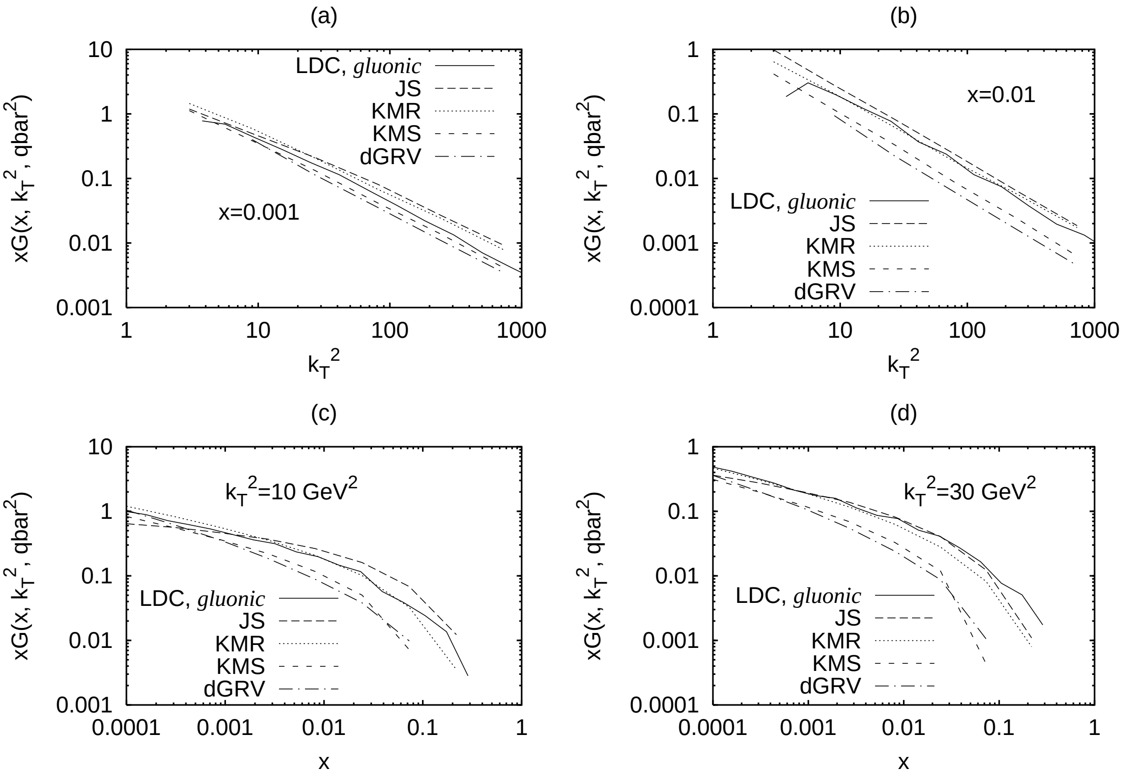

Figure 10: The LDC *gluonic* unintegrated gluon distribution function (full curve), compared to the corresponding results of JS (long-dashed curve), KMR (dotted curve), KMS (short-dashed curve) and dGRV (dash-dotted curve) as functions of $k_\perp^2$ for (a) $x = 0.001$ and (b) $x = 0.01$, and as functions of x for (c) $k_\perp^2 = 10\,\mathrm{GeV}^2$ and (d) $k_\perp^2 = 30\,\mathrm{GeV}^2$. Results for LDC, JS and KMR, with $\overline{q} = 2k_\perp$, are shown together with the 1-scaled distribution functions of KMS and dGRV.

relevant to study the CCFM distributions for $\overline{q}$ equal to the saturation value, rather than e.g. for $\overline{q} = k_\perp$. Indeed, for this larger $\overline{q}$-value we see in figure 8 that there is a rather good agreement between the three models.

This feature is further illustrated in figure 10, which shows the distribution functions for $\overline{q} = 2k_\perp$, as a functions of $k_\perp^2$ for fixed x and as a functions x for fixed $k_\perp^2$, and we see indeed a reasonable agreement between the LDC, JS, and KMR results, even if the JS result for $k_\perp^2 = 10\,\mathrm{GeV}^2$ lies somewhat above the other two for large x and below for smaller x-values. In these figures we also show the single scale KMS and dGRV results. Although these earlier parameterizations are somewhat lower for larger x-values, we note a fair overall agreement between all five models.

5. Summary

Unintegrated parton distribution functions are not uniquely defined. They are not experimental observables, and their definition and properties depend critically on the formalism used. Thus when calculating e.g. cross-sections for production of jets or heavy quarks it

JHEP09(2002)005

is necessary to use a consistent formalism for off-shell parton cross-sections and parton distribution functions.

In this paper we present results for integrated and unintegrated gluon distribution functions according to the definitions in the Linked Dipole Chain model, obtained from the LDCMC program. We compare them with those obtained in other formalisms, in particular with results from the CCFM model obtained from the SMALLX and CASCADE MCs, and we demonstrate how to make a relevant comparison between the models. Indeed we find in this way a reasonable agreement between distributions obtained in different formalisms.

Adjusting the input distribution functions for $k_\perp = k_{\perp 0}$, it is possible to find a good fit to the structure function F_2 from LDCMC. The corresponding integrated gluon distribution function agrees well with fits to more complete data sets obtained by the CTEQ or MRST collaborations. The result is rather insensitive to non-singular contributions in the gluon splitting function or from quark links in the chain. The contributions from quarks can be almost fully compensated by adjusting the input distribution functions. Omitting the non-singular terms in the gluon splitting function has a somewhat larger effect, reducing the gluon distribution for small x by roughly a factor 2.

In the CCFM formalism the unintegrated parton distribution functions depend sensitively on two different scales: $k_\perp$, which specifies the transverse momentum and the virtuality of the interacting parton, and $\overline{q}$, which determines an angle beyond which there is no (quasi-)real parton in the chain of initial-state radiation. Many of the gluons which make up the initial-radiation chain in the CCFM model are treated as final-state radiation in the LDC formalism. Therefore typical z-values are smaller in LDC, and most of the problem of angular ordering is postponed to the treatment of the final-state radiation. This implies that in the LDC formalism the gluon distribution function is much less sensitive to the second scale $\overline{q}$, and to leading $\log 1/x$ it depends only on a single scale $k_\perp$.

In a typical hard sub-collision the relevant additional scale $\overline{q}$ should be given by $\overline{q}^2 \sim |\hat{t}|$ or $\hat{s}$. We observe that in the CCFM formalism, for a fixed $k_\perp$, the gluon distribution function saturates for $\overline{q} \gtrsim 2k_\perp$, before it falls off for larger $\overline{q}$-values. This corresponds to typical values of $\hat{t}$ or $\hat{s}$, and we therefore suggest that for a relevant comparison between the different formalisms we should choose $\overline{q}$ in this saturation region. Here we find indeed a reasonable agreement, not only between LDC and CCFM, but also with e.g. the two-scale formalism presented by Kimber, Martin and Ryskin, and the one-scale formalism by Kwiecinski, Martin and Sutton. Actually we see that it also agrees rather well with the derivative of the integrated distribution function GRV98, obtained in the pure DGLAP formalism.

Acknowledgments

We want to thank Hannes Jung for valuable discussions, and in particular for help in evaluating the distribution functions for the JS, KMS, and KMR models.

JHEP09(2002)005

References

[1] V.N. Gribov and L.N. Lipatov, *Deep inelastic e p scattering in perturbation theory*, *Yad. Fiz.* **15** (1972) 781.

[2] L.N. Lipatov, *The parton model and perturbation theory*, *Sov. J. Nucl. Phys.* **20** (1975) 94.

[3] G. Altarelli and G. Parisi, *Asymptotic freedom in parton language*, *Nucl. Phys.* **B 126** (1977) 298.

[4] Y.L. Dokshitzer, *Calculation of the structure functions for deep inelastic scattering and* e^+e^- *annihilation by perturbation theory in quantum chromodynamics. (In russian)*, *Sov. Phys. JETP* **46** (1977) 641.

[5] Small x collaboration, B. Anderson et al., *Small x phenomenology: summary and status*, hep-ph/0204115.

[6] E.A. Kuraev, L.N. Lipatov and V.S. Fadin, *The Pomeranchuk singularity in nonabelian gauge theories*, *Sov. Phys. JETP* **45** (1977) 199.

[7] I.I. Balitsky and L.N. Lipatov, *The Pomeranchuk singularity in quantum chromodynamics*, *Sov. J. Nucl. Phys.* **28** (1978) 822.

[8] M. Ciafaloni, *Coherence effects in initial jets at small* Q^2/s, *Nucl. Phys.* **B 296** (1988) 49.

[9] S. Catani, F. Fiorani and G. Marchesini, *QCD coherence in initial state radiation*, *Phys. Lett.* **B 234** (1990) 339.

[10] B. Andersson, G. Gustafson and J. Samuelsson, *The linked dipole chain model for DIS*, *Nucl. Phys.* **B 467** (1996) 443.

[11] B. Andersson, G. Gustafson and H. Kharraziha, *Investigations into the BFKL mechanism with a running QCD coupling*, *Phys. Rev.* **D 57** (1998) 5543 [hep-ph/9711403].

[12] G.P. Salam, *Soft emissions and the equivalence of BFKL and CCFM final states*, *J. High Energy Phys.* **03** (1999) 009 [hep-ph/9902324].

[13] G. Marchesini, *QCD coherence in the structure function and associated distributions at small x*, *Nucl. Phys.* **B 445** (1995) 49 [hep-ph/9412327].

[14] H. Kharraziha and L. Lonnblad, *The linked dipole chain Monte Carlo*, *J. High Energy Phys.* **03** (1998) 006 [hep-ph/9709424].

[15] M. Ciafaloni and G. Camici, *Energy scale(s) and next-to-leading BFKL equation*, *Phys. Lett.* **B 430** (1998) 349 [hep-ph/9803389].

[16] V.S. Fadin and L.N. Lipatov, *BFKL pomeron in the next-to-leading approximation*, *Phys. Lett.* **B 429** (1998) 127 [hep-ph/9802290].

[17] Y.L. Dokshitzer, V.A. Khoze, A.H. Mueller and S.I. Troyan, *Basics of perturbative QCD*. Ed. Frontières, Gif-sur-Yvette, France 1991.

[18] E.M. Levin and M.G. Ryskin, *High-energy hadron collisions in QCD*, *Phys. Rept.* **189** (1990) 267.

[19] J. Bartels and H. Lotter, *A note on the BFKL pomeron and the 'hot spot' cross-section*, *Phys. Lett.* **B 309** (1993) 400.

[20] J.R. Forshaw, P.N. Harriman and P.J. Sutton, *On the relevance of the BFKL equation to deep inelastic scattering at HERA*, *Nucl. Phys.* **B 416** (1994) 739.

JHEP09(2002)005

[21] J. Kwiecinski, A.D. Martin and P.J. Sutton, *Constraints on gluon evolution at small x*, *Z. Physik* **C 71** (1996) 585 [hep-ph/9602320].

[22] G. Marchesini and B.R. Webber, *Simulation of QCD initial state radiation at small x*, *Nucl. Phys.* **B 349** (1991) 617.

[23] G. Marchesini and B.R. Webber, *Final states in heavy quark leptoproduction at small x*, *Nucl. Phys.* **B 386** (1992) 215.

[24] H. Jung, *The CCFM Monte Carlo generator cascade*, *Comput. Phys. Commun.* **143** (2002) 100 [hep-ph/0109102].

[25] H. Kharraziha, private communication.

[26] G. Gustafson and G. Miu, *Minijets and transverse energy flow in high energy collisions*, *Phys. Rev.* **D 63** (2001) 034004 [hep-ph/0002278].

[27] G. Gustafson, L. Lönnblad, and G. Miu, preprint in preparation.

[28] Discussions with Y.L. Dokshitzer et al., *Lund workshop on small-x evolution*, Lund, June 2002. To be published in the proceedings.

[29] H. Jung and G.P. Salam, *Hadronic final state predictions from CCFM: the hadron-level Monte Carlo generator Cascade*, *Eur. Phys. J.* **C 19** (2001) 351 [hep-ph/0012143].

[30] J. Kwiecinski, A.D. Martin and A.M. Stasto, *A unified BFKL and glap description of F_2 data*, *Phys. Rev.* **D 56** (1997) 3991 [hep-ph/9703445].

[31] M.A. Kimber, A.D. Martin and M.G. Ryskin, *Unintegrated parton distributions*, *Phys. Rev.* **D 63** (2001) 114027 [hep-ph/0101348].

[32] M. Glück, E. Reya and A. Vogt, *Dynamical parton distributions revisited*, *Eur. Phys. J.* **C 5** (1998) 461 [hep-ph/9806404].

[33] H1 collaboration, S. Aid et al., *A measurement and QCD analysis of the proton structure function $f_2(x, q\ 2)$ at HERA*, *Nucl. Phys.* **B 470** (1996) 3 [hep-ex/9603004].

[34] ZEUS collaboration, M. Derrick et al., *Measurement of the f_2 structure function in deep inelastic e^+p scattering using 1994 data from the Zeus detector at HERA*, *Z. Physik* **C 72** (1996) 399 [hep-ex/9607002].

[35] New Muon collaboration, M. Arneodo et al., *Measurement of the proton and the deuteron structure functions, F_2^p and F_2^d*, *Phys. Lett.* **B 364** (1995) 107 [hep-ph/9509406].

[36] E665 collaboration, *Proton and deuteron structure functions in muon scattering at 470 GeV*, M.R. Adams et al., *Phys. Rev.* **D 54** (1996) 3006.

[37] V.N. Baier, E.A. Kuraev, V.S. Fadin and V.A. Khoze, *Inelastic processes in quantum electrodynamics at high-energies*, *Phys. Rept.* **78** (1981) 293.

[38] S. Catani, M. Ciafaloni and F. Hautmann, *High-energy factorization and small x heavy flavor production*, *Nucl. Phys.* **B 366** (1991) 135.

[39] CTEQ collaboration, H.L. Lai et al., *Global QCD analysis of parton structure of the nucleon: CTEQ5 parton distributions*, *Eur. Phys. J.* **C 12** (2000) 375 [hep-ph/9903282].

[40] A.D. Martin, R.G. Roberts, W.J. Stirling and R.S. Thorne, *MRST2001: partons and α_s from precise deep inelastic scattering and Tevatron jet data*, *Eur. Phys. J.* **C 23** (2002) 73 [hep-ph/0110215].